Catalysis Science & Technology

ROYAL SOCIETY OF CHEMISTRY

PAPER

View Article Online
View Journal | View Issue

Cite this: *Catal. Sci. Technol.*, 2020, **10**, 4405

pH universal Ru@N-doped carbon catalyst for efficient and fast hydrogen evolution†

Baocheng Zheng,[a] Li Ma,[a] Bing Li,[a] Dong Chen,[a] Xueliang Li,[a] Jianbo He,[a] Jianhui Xie,*[a] Marc Robert*[b] and Tai-Chu Lau*[c]

Received 17th December 2019,
Accepted 10th June 2020

DOI: 10.1039/c9cy02552a

rsc.li/catalysis

The development of efficient and cost-effective electrocatalysts for the hydrogen evolution reaction (HER) is of intense interest because H_2 is one of the most promising renewable energy sources. Herein, we report a highly efficient and stable HER electrocatalyst composed of ruthenium nanoparticles embedded in nitrogen-doped carbon (NC), which is synthesized *via* a simple thermolysis process using a ruthenium complex as metal precusor and using ethylenediaminetetraacetic acid tetrasodium (Na_4EDTA) salt as ligand and carbon source. It is found that the amount of Na_4EDTA employed plays an important role in achieving sutiable and uniform Ru nanoparticles. The resulting Ru@NC(1 : 5) was found to exhibit excellent HER activity and robust stability in alkaline media (1.0 M KOH) with a low overpotential at 10 mA cm^{-2} (29 mV), small Tafel slope (27 mV per decade) and a high turnover frequency (TOF) of 0.96 s^{-1} at an overpotential of 50 mV, which are comparable to the state-of-the-art commercial Pt/C catalyst. Based on the characterization of the samples and the electrochemical measurements, this high performance of Ru@NC(1 : 5) is ascribed to its smallest particle size (*ca.* 2.1 nm diameter), large active site density and the high electrochemical conductivity by the N-doped carbon support. In addition, Ru@NC(1 : 5) also works well in acidic media (0.5 M H_2SO_4) indicating it is a pH-universal catalyst.

1. Introduction

The hydrogen evolution reaction (HER) is a key step in overall water splitting; it stores energy by producing H_2 gas which is a green and sustainable alternative to fossil fuels.[1–3] Therefore, the employment of H_2 as an energy source in our real life has been attracting more and more attention in these years. Compared to the traditional H_2 production by steam reforming of natural gas, electrochemical reduction of water is much cleaner and more sustainable because the electricity consumed can be obtained from renewable energy sources such as solar, wind, river and so on.[4,5] Platinum (Pt) is known to be the most efficient electrocatalyst for HER in both acidic and alkaline solutions[6–8] owing in part to its appropriate Pt–H bond strength,[9] but the large-scale application of Pt HER electrocatalysis is impractical due to the high cost and low natural abundance of Pt.[10] Therefore, the search for more economical candidates is desirable. Much effort has been made to develop earth-abundant Pt-free HER catalysts.[11–15] Although the HER activity of some of these catalysts is comparable to that of Pt in acidic media, they are generally susceptible to corrosion in acid. In addition, most catalysts exhibit much lower activity and stability in alkaline media. Since many commercial water electrolysers operate in alkaline solutions, it is necessary to develop more stable and efficient catalysts under alkaline conditions.[16]

Recently, much attention has been paid to the use of ruthenium as HER electrocatalysts, since the metal–hydrogen bond strength of Ru is similar to that of Pt (~65 kcal mol^{-1}), but it is around 25 times cheaper than Pt.[17] There have been several reports suggesting that Ru is a promising and attractive alternative to Pt in achieving excellent HER performance.[16–24] In particular, a number of electrocatalysts based on Ru nanoparticles (NPs) have been recently shown to exhibit similar or even better HER performance compared to the Pt/C benchmark.[25–30] However, the preparation of Ru NPs usually requires a strong reducing reagent such as $NaBH_4$, and the direct loading of Ru NPs on the surface of the supports may be not enough to guarantee the sufficient interactions with the supports. Thermolysis of a Ru precursor with a carbon source seems to be a potential way for the

[a] *Anhui Province Key Laboratory of Advanced Catalytic Materials and Reaction Engineering, School of Chemistry and Chemical Engineering, Hefei University of Technology, Hefei 230009, People's Republic of China. E-mail: jianhuixie@hfut.edu.cn*
[b] *Université de Paris, Laboratoire d'Electrochimie Moléculaire, CNRS, F-75006 Paris, France. E-mail: robert@u-paris.fr*
[c] *Department of Chemistry, City University of Hong Kong, Tat Chee, Avenue, Kowloon Tong, Hong Kong, People's Republic of China. E-mail: bhtclau@cityu.edu.hk*

† Electronic supplementary information (ESI) available. See DOI: 10.1039/c9cy02552a

in situ generation of Ru NPs embedded in a carbon matrix, though it is still a challenge to control the uniform particle size and the homogenous distribution of NPs during the high temperature pyrolysis process. Herein, we report the design of a series of Ru-based HER electrocatalysts composed of uniform Ru nanoparticles embedded in N-doped carbon (NC) (Ru@NC). These electrocatalysts are prepared by pyrolysis of mixtures of a Ru precursor and various ratios of a carbon-containing ligand, and they are found to exhibit excellent activity and stability in alkaline solution as well as good performance in acidic media.

The synthetic route for Ru@NC is illustrated in Scheme 1. $Bu_4N[Ru(N)Cl_4]$ and Na_4EDTA (H_4EDTA = ethylenediamine tetraacetic acid) were chosen as the precursors because the chloro ligands of $[Ru(N)Cl_4]^-$ are relatively labile and can be readily substituted by EDTA to give $[Ru(N)(EDTA)_x]^{n-}$.[31] Thermolysis of $[Ru(N)(EDTA)_x]^{n-}$ at 850 °C under inert atmosphere affords Ru@NC. Various samples of Ru@NC were prepared by adjusting the mole ratio of $Bu_4N[Ru(N)Cl_4]$ and Na_4EDTA (1 : 2, 1 : 5, 1 : 10 and 1 : 20). N-Doped carbon without Ru as obtained by direct thermolysis of Na_4EDTA under similar conditions.

2. Experimental

2.1. Reagents

All chemicals were of reagent grade and used as received unless otherwise noted. $[Bu_4N[Ru(N)Cl_4]$ was prepared according to a literature method.[31] Water for the experiments was distilled twice from alkaline permanganate. Ethylenediaminetetraacetic acid tetrasodium (Na_4EDTA) and commercial Pt/C (20 wt%) catalyst were purchased from Sigma-Aldrich. Nafion solution (5% wt in water and 1-propanol) was purchased from Alfa Aesar.

2.2. Preparation of Ru@NC

The synthesis of Ru@NC electrocatalysts follows the same procedure. Take Ru@NC(1 : 5) for example. Typically, 500 mg $[Bu_4N[Ru(N)Cl_4]$ (1 mmol) and 1.9 g Na_4EDTA (5 mmol) were dissolved in a mixed solvent containing water (50 mL) and acetone (20 mL) and the solution was stirred for 15 min at room temperature. Then, the solution was evaporated under vacuum. The remaining solid was triturated followed by carbonization at 850 °C under N_2 atmosphere for 2 h. The final black powder was soaked in 0.5 M H_2SO_4 solution for one night followed by washing with water and absolute ethanol, and dried at vacuum for 12 h. Ru@NC(1 : 2, 1 : 10 and 1 : 20) were prepared by the similar procedure. N-Doped carbon without Ru was obtained by direct thermolysis of Na_4EDTA under the same conditions.

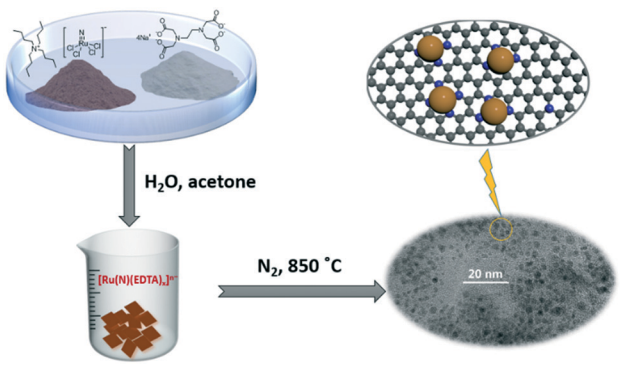

Scheme 1 Schematic illustration of the synthesis and the structure of the Ru@NC electrocatalysts.

2.3. Physical characterization

The X-ray diffractometer (X'Pert PRO MPD) with Cu-Kα radiation was employed to obtain the X-ray powder diffraction (XRD) with the 2-theta range from 10° to 90°. Scanning electron microscopy (SEM) images were recorded on a field-emission scanning electron microscope (JEM-2100F) with an accelerating voltage of 5 kV. The elemental mapping was analysed by the energy dispersion X-ray spectroscopy (EDS). Transmission electron microscopy (TEM) images were obtained on a SU8020 microscope. The surface area was obtained by nitrogen adsorption–desorption isotherms using the Brunauer–Emmett–Teller (BET) method on Autosorb-IQ3 sorption analyzer based on N_2 adsorption/desorption. The chemical elements and valence states of samples were investigated by X-ray photoelectron spectroscopy with an ESCALAB250Xi spectrometer and all data were corrected by employing the C 1s peak at 284.8 eV as an internal standard. Raman spectra were measured on a LabRAM HR Evolution in the range from 700 to 3000 cm^{-1}. The Ru contents of Ru@NC were determined by ICP-MS (ICAPQ).

2.4. Electrochemical measurements

The electrochemical experiments were performed on a CHI 660E instrument with a three-electrode configuration using glassy carbon (GC) electrode as working electrode, graphite rod as counter electrode and saturate calomel electrode (SCE) as reference electrode, respectively, at room temperature. For the preparation of working electrode, the GC electrode of 3 mm diameter was initially polished with a 0.05 mm alumina powder followed by washing with water and acetone. Then, 3.1 mg of catalyst and 100 μL of 5 wt% Nafion solution were dispersed in 0.9 mL methanol followed by 10 min sonication to obtain a homogeneous ink. Finally, 5 μ L of the catalyst ink was loaded onto the cleaned glassy carbon electrode and dried at room temperature, which led to a catalyst loading of 0.22 mg cm^{-2}. The potentials of HER in all figures were regulated by reversible hydrogen electrode (RHE) using the equation: $E_{RHE} = E_{SCE} + 0.24 + 0.059$ pH. The electrochemical stability tests were carried out by performing 3000 CV cycles in the potential range of 0.1 to −0.2 V *vs.* RHE at a scan rate of 50 mV s^{-1}. The electrochemical impedance spectroscopy (EIS) analyses were measured in the frequency range from 0.01 to 100 000 Hz and with an amplitude of 10 mV. Faradaic efficiency was calculated by the equation: Faradaic efficiency

= $2nF/Q$, where n is the amount of H_2 collected by the water drainage method and calculated using the gas laws; Q is the amount of charge calculated from the corresponding i–t curve.

2.5. Determination of the active site density of Ru@NC(1 : 5)

The active site density was measured by the Cu under-potential deposition method (UPD), which means that the active sites responsible for the proton reduction, are same to those for the reduction of Cu^{2+} at an underpotential.[32] The detailed procedure is as follows. Initially, the CVs of the prepared electrode containing NC or Ru@NC(1 : 5) were measured in 0.1 M H_2SO_4 as baseline. Then the electrodes were polarized at 0 V *vs.* RHE for 100 s in a solution containing 0.1 M H_2SO_4 and 20 mM $CuSO_4$ to deposit Cu. After that, the CV measurements of the electrodes with deposited copper were performed in the same mixed solution (0.1 M H_2SO_4 and 20 mM $CuSO_4$) from the initial 0 V *vs.* RHE to a point where all of the deposited copper had been oxidized at a scan rate of 0.01 V s^{-1}. The observation of only one reduction peak or oxidation peak indicates the overlap of UPD Cu and overpotential deposition (OPD) Cu. Therefore, chloride ion was employed to separate the UPD and OPD peaks.[28] The procedure of the CV measurements is similar except that the electrolyte contains 0.1 M H_2SO_4, 20 mM $CuSO_4$ and 60 mM NaCl (Fig. S18, ESI†). Charges of oxidative copper stripping were corrected by subtracting the charge obtained for the same electrode in 0.1 M H_2SO_4. The active site density of the prepared electrode was calculated by the equation: active site density = $QL/(2FA)$, where Q is amount of charges of copper stripping from the current–potential curve; L is Avogadro constant; F is Faraday's constant and A is the surface area of the working electrode. The active site density is calculated to be 8.26×10^{16} cm^{-2}.

3. Results and discussion

3.1. Morphology and structure characterization

The morphology and detailed structures of Ru@NC catalysts were initially investigated by scanning electron microscopy (SEM) and transmission electron microscopy (TEM). The SEM image of Ru@NC(1 : 5) (Fig. 1a) shows that the catalyst consists of many small sheets. The corresponding energy dispersive spectroscopy (EDS) reveals the presence and homogeneous distribution of Ru, C and N elements and the Ru content was further detected to be 36% wt% by SEM-EDS (Fig. S4, ESI†), which is in good agreement with the value of 36.3% wt% obtained by ICP-MS. The Ru contents of Ru@NC(1 : 2, 1 : 10, 1 : 20) were also investigated by ICP-MS and were found to be 21.7% wt%, 19.2% wt% and 9.4% wt%, respectively (Table 1). The TEM image of Ru@NC(1 : 5) in Fig. 1b clearly shows that the Ru nanoparticles are homogeneously distributed on the carbon skeleton as dark spots with uniform size distribution (average diameter *ca.* 2.1 nm) (Fig. 1c). The particle size of Ru@NC(1 : 2, 1 : 10 and 1 : 20) were found to be the 4.2 nm, 3.8 nm and 4.5 nm, respectively (Fig. S1–S3, ESI†). Intriguingly, Ru@NC(1 : 5) has

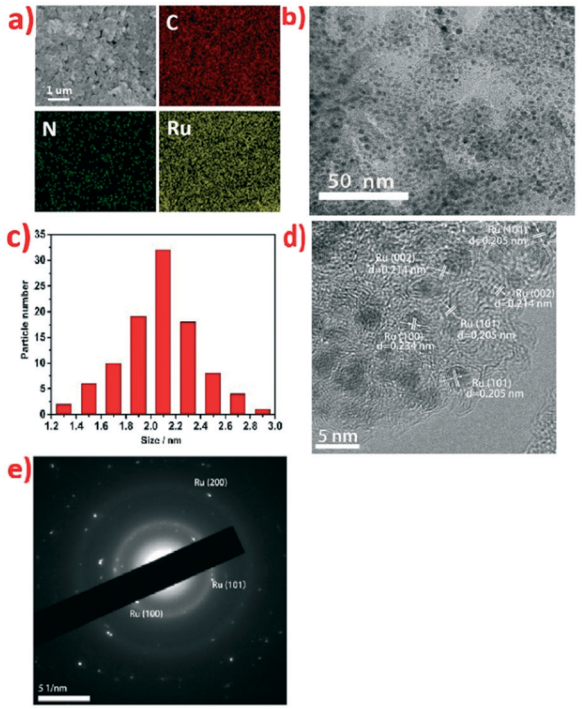

Fig. 1 Morphology and physical characterization of Ru@NC(1 : 5). a) SEM image and corresponding EDS mapping images of C, N and Ru. b) TEM image. c) The corresponding particle size distribution of the Ru nanoparticles. d) HRTEM image. e) Selected-area electron diffraction (SAED) pattern.

the most abundant Ru content but smallest particle size. The high resolution TEM (HRTEM) image of Ru@NC(1 : 5) (Fig. 1d) further reveals the embedding of Ru NPs on the carbon skeleton. The spacing of the crystal lattices 0.205 nm, 0.214 nm and 0.234 nm can be attributed to the (101), (002) and (100) planes of hexagonal Ru, respectively.

The structures of the Ru@NC samples were further confirmed by X-ray powder diffraction (XRD). For Ru@NC(1 : 5), the indicated peaks in Fig. 2a can be attributed to hexagonal Ru (PCPDF no. 06-0663), while a small diffraction peak of graphite (002) plane was observed at 26.7°. The XRD patterns of Ru@NC(1 : 2, 1 : 10 and 1 : 20) suggest the same compositions (Fig. S8, ESI†). X-ray photoelectron spectroscopy (XPS) was also performed to identify the binding states and quantitative chemical compositions of Ru@NC. The XPS spectra of Ru@NC(1 : 5) (Fig. 2) and Ru@NC(1 : 2, 1 : 10 and 1 : 20) (Fig. S9–S11, ESI†) clearly indicate the presence of C, N, O and Ru elements. The occurrence of the O peak is presumably due to the physically

Table 1 Ru content by ICP analysis and average particle diameter of Ru@NC catalysts

Catalysts	Ru content/wt%	Average diameter/nm
Ru@NC(1 : 5)	36.3	2.1
Ru@NC(1 : 2)	21.7	4.2
Ru@NC(1 : 10)	19.2	3.8
Ru@NC(1 : 20)	9.4	4.5

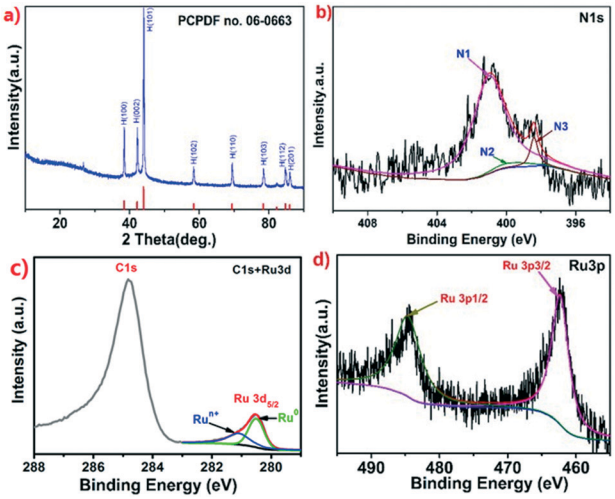

Fig. 2 XRD and XPS analysis of Ru@NC(1 : 5). a) XRD pattern. b) High-resolution XPS spectrum of N 1s. c) High-resolution XPS spectrum of C 1s and Ru 3d. (d) High-resolution XPS spectrum of Ru 3p.

adsorbed oxygen or edge oxygen of carbon matrix. For Ru@NC(1 : 5), the bonding configurations of N and Ru in the sample were further studied. The N 1s XPS spectrum (Fig. 2b) reveals three peaks at 398.4, 399.5 and 400.9 eV, which can be assigned to pyridinic N (N3), pyrrolic N, (N2) and graphitic N (N1), respectively. Furthermore, 90% N belongs to graphitic N which is reported to be able to activate the adjacent C atoms to increase the density of active sites.[33] Although pyridinic N and pyrrolic N can coordinate to metal, they can also block active sites of metal NPs.[26] Therefore, too many pyridinic N and pyrrolic N are not desirable. The binding energies of Ru 3d, Ru 3p3/2 and Ru 3p1/2 are observed at 280.5 eV, 462.1 and 484.1 eV, respectively, indicating the presence of metallic Ru^0 and Ru^{n+} species (Fig. 2c and d). Because Ru 3d3/2 at 284.5 eV is overlapped with C 1s signal, the composition of Ru was only investigated by the Ru 3d5/2 XPS signal. The peak located at 280.3 eV is assigned to Ru^0 and the rest is assigned to electron-deficient Ru^{n+} species.[34] The Ru^0/Ru^{n+} ratio was calculated from the integral peaks area of fitted Ru^0 and Ru^{n+} species which are found to be 1.26, 1.31, 1.35 and 1.71 for Ru@NC(1 : 2, 1 : 5, 1 : 10, 1 : 20), respectively. Based on the overall Ru contents of ICP analysis, the Ru^0 contents of Ru@NC(1 : 2, 1 : 5, 1 : 10, 1 : 20) are 12.1% wt, 20.6% wt, 11.0% wt and 5.9% wt, respectively. The carbon component of Ru@NC(1 : 5) was further investigated by Raman spectroscopy (Fig. S12, ESI†). A typical D-band at 1358 cm^{-1} and a typical G-band at 1600 cm^{-1} are observed with the intensity ratio (I_D/I_G) of 0.978, indicating a highly disordered and defective graphitic carbon component.[35]

3.2. Electrocatalytic performance of Ru@NC for HER

The electrocatalytic activity for HER by Ru@NC was initially investigated in alkaline solution (1.0 M KOH). For comparison, catalysis by the commercial Pt/C (20 wt%) benchmark was also measured under the same conditions.[36]

The HER catalytic activity of Pt catalysts is excellent in alkaline electrolytes because the energy barrier of the Volmer step is so low that the rate of HER process is determined by a fast Tafel step.[24,37] Similarly, Ru has been shown to have good water dissociation ability,[38] which may also make the Volmer step of electrocatalytic HER facile in alkaline solutions.[39] As shown by the polarization curves of Ru@NC catalysts without iR correction in Fig. 3a, all the catalysts exhibit distinctly positive electrocatalytic HER performance. Among the prepared catalysts, Ru@NC(1 : 5) shows the best activity, which is comparable to that of the Pt/C benchmark, probably owing to its smallest particle size. Although the other Ru@NC catalysts also contain a few of small Ru NPs, it is insufficient due to the much lower Ru content than that of Ru@NC(1 : 5) as aforementioned. Both Ru@NC(1 : 5) and Pt/C show very small onset overpotentials (η) with η_0 = 0 mV. When the current density reaches 10 mA cm^{-2}, the overpotential for Ru@NC(1 : 5) is only 29 mV, which is very close to that of the Pt/C benchmark (η_{10} = 27 mV). Furthermore, Tafel plots obtained from the corresponding polarization curves were used to examine the kinetics during the HER process. The Tafel slope for Ru@NC(1 : 5) is approximately 27 mV per decade (Fig. 3b), which is similar to that of Pt/C benchmark (25 mV per decade), suggesting that the HER process occurs *via* Volmer–Tafel mechanism (30 mV per decade) in which the combination of two chemisorbed hydrogen atoms is the rate-determining step. Overall, the above results clearly indicate that Ru@NC(1 : 5) is a highly efficient electrocatalyst for HER in alkaline media and is comparable to the other excellent Ru-based electrocatalysts (Table 2).[19,21,23,26–30,39]

The other important criterion of a good catalyst is the stability during the catalytic process. Therefore, we carried out a long-term durability test of Ru@NC(1 : 5) using cyclic voltammetry (CV) initially. The linear sweep voltammetry

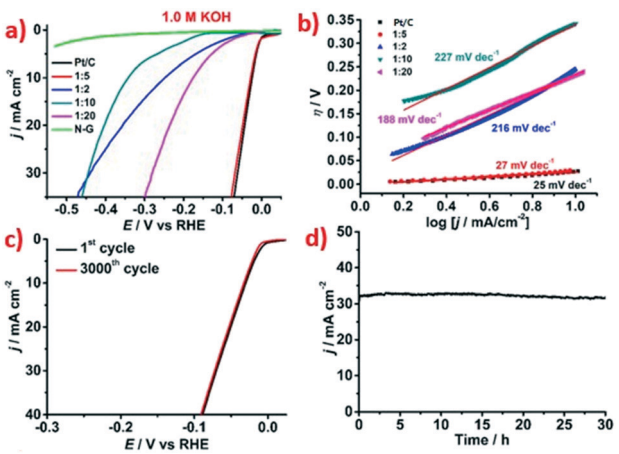

Fig. 3 a) HER polarization curves of Ru@NC (1 : 2, 1 : 5, 1 : 10, 1 : 20), NC and Pt/C in 1.0 M KOH at a scan rate of 5 mV s^{-1}. b) Corresponding Tafel plots. c) HER polarization curves recorded before and after 3000 CV cycles for Ru@NC(1 : 5). d) Time-dependent current density curve for Ru@NC(1 : 5) in 0.5 M H_2SO_4 at a constant potential of −0.088 V *vs.* RHE for 30 h.

Table 2 Recently reported HER electrocatalysts in alkaline and acidic electrolytes

Catalyst	Loading amount/mg cm^{-2}	Electrolyte	Current density/mA cm^{-2}	Overpotential at corresponding j/mV	Tafel slope/mV per decade	References
Ru@NC	0.22	1 M KOH	10	29	27	This work
		0.5 M H_2SO_4		62	40	
R–TiO_2:Ru	0.255	1 M KOH	10	150	95	19
Ru@C_2N	0.285	1 M KOH	10	17	38	21
		0.5 M H_2SO_4		22	30	
RuP_2@NPC	1.0	1 M KOH	10	52	69	23
		0.5 M H_2SO_4		38	38	
Ru@GnP	0.25	1 M KOH	10	22	28	26
		0.5 M H_2SO_4		13	30	
Ru@NC	—	1 M KOH	10	26	36	27
Ru@CN	0.247	1 M KOH	10	32	53	28
		0.5 M H_2SO_4		126	—	
Ru/MWCNTs	0.28	1 M KOH	10	39	28	29
Ru/C-300	—	1 M KOH	10	14	32.5	30
RuCo alloy	0.275	1 M KOH	10	28	31	39
Ru-CCS	0.285	0.5 M H_2SO_4	10	27.3	33	40
Ni@Ni2P–Ru	0.283	0.5 M H_2SO_4	10	51	35	41
Ru^0/CeO_2	0.197	0.5 M H_2SO_4	10	47	41	42
P–W_2C@NC	3.5	0.5 M H_2SO4	10	89	53	44

(LSV) curves were measured before and after 3000 CV cycles at a scan rate of 50 mV s^{-1} (Fig. 3c), and the LSV of 3000th cycle remains almost the same as that of the first cycle. Then, we further evaluated the durability of the Ru@NC(1 : 5) electrocatalyst by electrolysis at a fixed potential of −0.074 V *vs.* RHE. As shown in Fig. 3d, although the current density reaches up to *ca.* 32 mA cm^{-2} at this potential, it is maintained for 30 h with negligible decrease. These results reveal the excellent stability of Ru@NC(1 : 5) which is better than that of Pt/C (Fig. S15, ESI†). The TEM image of the catalyst after the durability test (Fig. S13, ESI†) shows that the morphology and structure are similar to that of the fresh catalyst. The EDS image reveals a 34.86 wt% Ru content (Fig. S14, ESI†), which is very close to 36 wt% of the fresh catalyst, suggesting little metal loss after the long term test, which may account for the excellent stability of Ru@NC(1 : 5). Furthermore, the amount of H_2 generated in the cathodic compartment matches well with the theoretical value, suggesting nearly a 100% Faradaic efficiency for Ru@NC(1 : 5) (Fig. S16, ESI†). Due to the high content of Ru@NC(1 : 5), the mass activity at an overpotential of 50 mV was found to be only 0.32 A $mgRu^{-1}$. To reach to the same mass activity, the overpotentials of Ru@NC(1 : 2, 1 : 10, 1 : 20) have to be 312 mV, 370 mV and 148 mV, respectively. Furthermore, the active site density of Ru@NC(1 : 5) was estimated to be as large as 8.26×10^{16} sites per cm^2 by the Cu under-potential deposition method (UPD) (Fig. S18, ESI†). The high active site density of Ru@NC(1 : 5) is probably due to its high Ru content and its small particle size. Finally, the H_2 turnover frequency (TOF = the number of H_2 molecules generated per second per active site), was found to be a 0.96 s^{-1} at an overpotential of 50 mV.

In view of the fact that other types of electrolytic cells such as proton exchange membrane electrolytic cell may work in acidic electrolyte during water splitting, we also investigated the HER electrocatalytic performance of the Ru@NC catalysts in acidic media (0.5 M H_2SO_4). Similarly, Ru@NC(1 : 5) exhibits the best HER activity in acidic electrolytes as shown in Fig. 4a. Under acidic conditions, both Ru@NC(1 : 5) and Pt/C show very small onset overpotentials (η) with η_0 = 17 mV and 8 mV, respectively. The overpotential η_{10} of Ru@NC(1 : 5) is 62 mV and the Tafel slope is approximately 40 mV per decade, slightly larger than that of the Pt/C benchmark (Fig. 4b). However, the LSV curve of Ru@NC(1 : 5) measured after 3000 CV cycles (Fig. 4c) is very similar to that of the first cycle suggesting the good stability of Ru@NC(1 : 5) in acidic media. The long-term durability test of Ru@NC(1 : 5) (Fig. 4d) shows negligible degradation for over 30 h under acidic conditions, superior to that of Pt/C (Fig. S15, ESI†). In addition, the Faradic efficiency is found

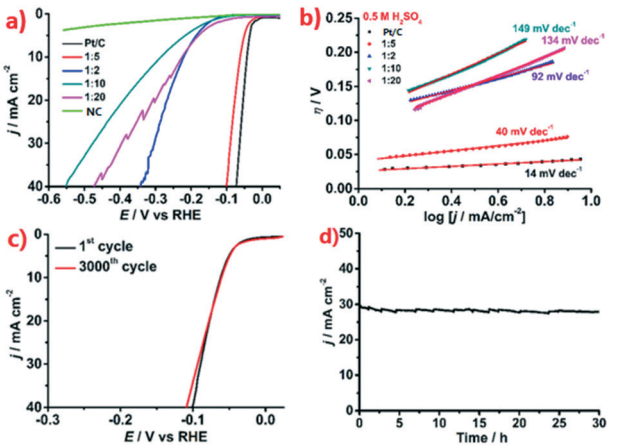

Fig. 4 a) HER polarization curves of Ru@NC (1 : 2, 1 : 5, 1 : 10, 1 : 20), NC and Pt/C in 0.5 M H_2SO_4 at a scan rate of 5 mV s^{-1}. b) Corresponding Tafel plots. c) HER polarization curves recorded before and after 3000 CV cycles for Ru@NC(1 : 5). d) Time-dependent current density curve for Ru@NC(1 : 5) in 0.5 M H_2SO_4 at a constant potential of −0.088 V *vs.* RHE for 30 h.

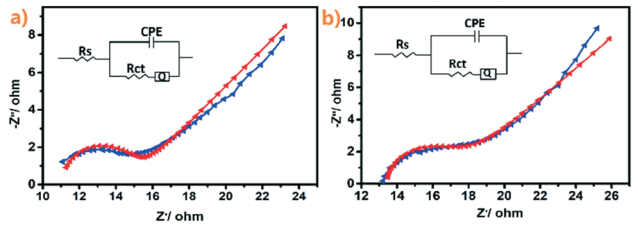

Fig. 5 a) Measured (blue) and fitted (red) Nyquist plots of Ru@NC(1 : 5) in 0.5 M H_2SO_4 at a constant potential of −0.088 V *vs.* RHE. b) Measured (blue) and fitted (red) Nyquist plots of Ru@NC(1 : 5) in 1.0 M KOH at a constant potential of −0.074 V *vs.* RHE.

to be almost 100% as well (Fig. S17, ESI†) and the H_2 TOF is found to be a 0.64 s^{-1} at an overpotential of 50 mV. These results reveal that Ru@NC(1 : 5) possesses remarkable HER activity and stability in acidic media, which are close to some excellent examples of Ru-based catalysts and better than non-noble metal catalysts (Table 2).[20,21,23,26,28,40–43] More importantly, it suggests Ru@NC(1 : 5) can function well in both alkaline and acidic conditions.

In order to get more insight into the high electrocatalytic activity of Ru@NC in HER, the electrochemically active surface area (ECSA) of Ru@NC(1 : 2, 1 : 5, 1 : 10 and 1 : 20) was evaluated by the double-layered capacitance (Cdl) at non-Faraday area using the cyclic voltammetry (CV) method (Fig. S19, ESI†). Obviously, Ru@NC(1 : 5) exhibits a larger Cdl of 25.3 mF cm^{-2} than Ru@NC(1 : 2) (13.7 mF cm^{-2}), Ru@NC(1 : 10) (21.3 mF cm^{-2}) and Ru@NC(1 : 20) (22.5 mF cm^{-2}), indicating Ru@NC(1 : 5) benefits from the more exposed active sites. EIS measurements were also carried out to investigate the charge transfer between the interfaces of catalysts and electrolytes. As simulated with the equivalent circuits in Fig. 5, the obtained charge transfer resistances (R_{ct}) of Ru@NC(1 : 5) by Nyquist plots are found to be 38 Ω and 37 Ω in acidic and alkaline solutions, respectively, which are even smaller than that of Ru@NC (43.7 Ω)[21] and that of Ru-NGC (70 Ω),[45] indicating that the charge-transfer during the HER process is fast and favourable. This high electrochemical conductivity may be owing to the synergistic effects between the Ru NPs and the carbon support that facilitates the electron transfer between the catalyst and electrolyte interfaces. On the other hand, the support material is known to play an important role in stabilizing the metal nanoparticles. Carbon with a high degree of graphitization is a very stable and robust kind of support.[46] The strong interaction of Ru NPs with N-doped carbon can avoid either the detachment or the agglomeration of the Ru nanoparticles and thus improves the stability of the whole catalyst. Additionally, N_2 adsorption–desorption analysis was carried out to investigate the texture structure of Ru@NC(1 : 5). As shown in Fig. 6, Ru@NC(1 : 5) has a typical type II N_2 adsorption isotherm revealing a large specific surface area (298.69 m^2 g^{-1}) and a pore volume of 0.2295 cm^3 g^{-1} with an average pore diameter of 3.07 nm. The large specific surface area and the hierarchical pores can play a key role in ensuring the efficient dispersion of Ru NPs and contributing to the high active site density of the catalyst.

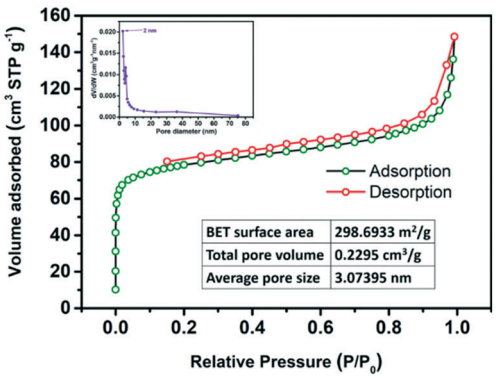

Fig. 6 N_2 adsorption/desorption isotherms of Ru@NC(1 : 5). Top inset: Corresponding pore size distribution.

Conclusions

In summary, we have successfully synthesized a series of HER electrocatalysts composed of Ru nanoparticles embedded in N-doped carbon by a simple process using $Bu_4N[Ru(N)Cl_4]$ and Na_4EDTA as precursors. By varying the molar ratio, Ru@NC(1 : 5) with particle size of *ca.* 2.1 nm diameter was found to exhibit the best HER activity in both acidic and alkaline media, which are comparable to the state-of-the-art Pt/C catalysts. Furthermore, this catalyst exhibits excellent stability during electrocatalytic HER in both strongly acidic and alkaline conditions. The experimental results suggest that the suitable particle size of Ru NPs, the high active site density and its synergistic effects with N-doped carbon support all contribute to the high electrocatalytic activity and stability.

Conflicts of interest

There are no conflicts to declare.

Acknowledgements

The work described in this paper was supported by the National Natural Science Foundation of China (Grant No. 21801058), the Anhui Provincial Natural Science Foundation (Grant No. 1808085QB28) and the Research Grants Council of Hong Kong (CityU 11301618). Partial financial support to M. R. from the Institut Universitaire de France (IUF) is gratefully acknowledged.

Notes and references

1 N. S. Lewis and D. G. Nocera, *Proc. Natl. Acad. Sci. U. S. A.*, 2006, **103**, 15729–15735.
2 J. Turner, G. Sverdrup, M. K. Mann, P.-C. Maness, B. Kroposki, M. Ghirardi, R. J. Evans and D. Blake, *Int. J. Energy Res.*, 2008, **32**, 379–407.

3 G. W. Crabtree, M. S. Dresselhaus and M. V. Buchanan, *Phys. Today*, 2004, **57**, 39–44.
4 M. S. Dresselhaus and I. L. Thomas, *Nature*, 2001, **414**, 332–337.
5 J. A. Turner, *Science*, 2004, **305**, 972.
6 E. J. Popczun, J. R. McKone, C. G. Read, A. J. Biacchi, A. M. Wiltrout, N. S. Lewis and R. E. Schaak, *J. Am. Chem. Soc.*, 2013, **135**, 9267–9270.
7 X. Bao, Y. Gong, Y. Chen, H. Zhang, Z. Wang, S. Mao, L. Xie, Z. Jiang and Y. Wang, *J. Mater. Chem. A*, 2019, **7**, 11038–11043.
8 X. Bao, J. Wang, X. Lian, H. Jin, S. Wang and Y. Wang, *J. Mater. Chem. A*, 2017, **5**, 16249–16254.
9 A. Gross, S. Schnur, E. Santos and W. Schmickler, *Catalysis in Electrochemistry:From Fundamental Aspects to Strategies for Fuel Cell Development*, Wiley, 2011.
10 R. B. Gordon, M. Bertram and T. E. Graedel, *Proc. Natl. Acad. Sci. U. S. A.*, 2006, **103**, 1209–1214.
11 J. Shan, T. Ling, K. Davey, Y. Zheng and S.-Z. Qiao, *Adv. Mater.*, 2019, **31**, 1900510.
12 T. Tian, L. Huang, L. H. Ai and J. Jiang, *J. Mater. Chem. A*, 2017, **5**, 20985–20992.
13 L. Liao, S. Wang, J. Xiao, X. Bian, Y. Zhang, M. D. Scanlon, X. Hu, Y. Tang, B. Liu and H. H. Girault, *Energy Environ. Sci.*, 2014, **7**, 387–392.
14 X. Feng, H. Wang, X. Bo and L. Guo, *ACS Appl. Mater. Interfaces*, 2019, **11**, 8018–8024.
15 P. Jiang, Q. Liu, Y. Liang, J. Tian, A. M. Asiri and X. Sun, *Angew. Chem., Int. Ed.*, 2014, **53**, 12855–12859.
16 J. Chen, H. Wang, Y. Gong and Y. Wang, *J. Mater. Chem. A*, 2019, **7**, 11038–11043.
17 Z.-F. Huang, J. Song, K. Li, M. Tahir, Y.-T. Wang, L. Pan, L. Wang, X. Zhang and J.-J. Zou, *J. Am. Chem. Soc.*, 2016, **138**, 1359–1365.
18 Y. Zheng, Y. Jiao, Y. Zhu, L. H. Li, Y. Han, Y. Chen, M. Jaroniec and S.-Z. Qiao, *J. Am. Chem. Soc.*, 2016, **138**, 16174–16181.
19 S. Nong, W. Dong, J. Yin, B. Dong, Y. Lu, X. Yuan, X. Wang, K. Bu, M. Chen, S. Jiang, L.-M. Liu, M. Sui and F. Huang, *J. Am. Chem. Soc.*, 2018, **140**, 5719–5727.
20 J. Yang, B. Chen, X. Liu, W. Liu, Z. Li, J. Dong, W. Chen, W. Yan, T. Yao, X. Duan, Y. Wu and Y. Li, *Angew. Chem., Int. Ed.*, 2018, **57**, 9495–9500.
21 J. Mahmood, F. Li, S.-M. Jung, M. S. Okyay, I. Ahmad, S.-J. Kim, N. Park, H. Y. Jeong and J.-B. Baek, *Nat. Nanotechnol.*, 2017, **12**, 441–446.
22 J. Xu, T. Liu, J. Li, B. Li, Y. Liu, B. Zhang, D. Xiong, I. Amorim, W. Li and L. Liu, *Energy Environ. Sci.*, 2018, **11**, 1819–1827.
23 Z. Pu, I. S. Amiinu, Z. Kou, W. Li and S. Mu, *Angew. Chem., Int. Ed.*, 2017, **56**, 11559–11564.
24 J. Creus, J. De Tovar, N. Romero, J. Garcia-Anton, K. Philippot, R. Bofill and X. Sala, *ChemSusChem*, 2019, **12**, 2493–2514.
25 J. Creus, S. Drouet, S. Surinach, P. Lecante, V. Colliere, R. Poteau, K. Philippot, J. Garcia-Anton and X. Sala, *ACS Catal.*, 2018, **8**, 11094–11102.
26 F. Li, G.-F. Han, H.-J. Noh, I. Ahmad, I.-Y. Jeon and J.-B. Baek, *Adv. Mater.*, 2018, 1803676.
27 Z.-L. Wang, K. Sun, J. Henzie, X. Hao, C. Li, T. Takei, Y.-M. Kang and Y. Yamauchi, *Angew. Chem., Int. Ed.*, 2018, **57**, 5848–5852.
28 J. Wang, Z. Wei, S. Mao, H. Li and Y. Wang, *Energy Environ. Sci.*, 2018, **11**, 800–806.
29 W. Gou, J. Li, W. Gao, Z. Xia, S. Zhang and Y. Ma, *ChemCatChem*, 2019, **11**, 1970–1976.
30 C. Xu, M. Ming, Q. Wang, C. Yang, G. Fan, Y. Wang, D. Gao, J. Bi and Y. Zhang, *J. Mater. Chem. A*, 2018, **6**, 14380–14386.
31 W. L. Man, T. M. Tang, T. W. Wong, T. C. Lau, S. M. Peng and W. T. Wong, *J. Am. Chem. Soc.*, 2004, **126**, 478–479.
32 C. L. Green and A. Kucernak, *J. Phys. Chem. B*, 2002, **106**, 1036–1047.
33 Y. Zheng, Y. Jiao, L. H. Li, T. Xing, Y. Chen, M. Jaroniec and S. Z. Qiao, *ACS Nano*, 2014, **8**, 5290–5296.
34 J. Ftouni, A. Munoz-Murillo, A. Goryachev, J. P. Hofmann, E. J. M. Hensen, L. Lu, C. J. Kiely, P. C. A. Bruijnincx and B. M. Weckhuysen, *ACS Catal.*, 2016, **6**, 5462–5472.
35 X.-H. Li, S. Kurasch, U. Kaiser and M. Antonietti, *Angew. Chem., Int. Ed.*, 2012, **51**, 9689–9692.
36 R. Subbaraman, D. Tripkovic, D. Strmcnik, K.-C. Chang, M. Uchimura, A. P. Paulikas, V. Stamenkovic and N. M. Markovic, *Science*, 2011, **334**, 1256–1260.
37 J. L. C. Fajin, M. N. D. S. Cordeiro and J. R. B. Gomes, *J. Phys. Chem. A*, 2014, **118**, 5832–5840.
38 Y. Zheng, Y. Jiao, A. Vasileff and S.-Z. Qiao, *Angew. Chem., Int. Ed.*, 2018, **57**, 7568–7579.
39 J. Su, Y. Yang, G. Xia, J. Chen, P. Jiang and Q. Chen, *Nat. Commun.*, 2017, **8**, 16029–16038.
40 D. Luo, B. Zhou, Z. Li, X. Qin, Y. Wen, D. Shi, Q. Lu, M. Yang, H. Zhou and Y. Liu, *J. Mater. Chem. A*, 2018, **6**, 2311–2317.
41 Y. Liu, S. Liu, Y. Wang, Q. Zhang, L. Gu, S. Zhao, D. Xu, Y. Li, J. Bao and Z. Dai, *J. Am. Chem. Soc.*, 2018, **140**, 2731–2734.
42 E. Demir, S. Akbayrak, A. M. Onal and S. Ozkar, *ACS Appl. Mater. Interfaces*, 2018, **10**, 6299–6308.
43 J. Yu, Q. He, G. Yang, W. Zhou, Z. Shao and M. Ni, *ACS Catal.*, 2019, **9**, 9973–10011.
44 G. Yan, C. Wu, H. Tan, X. Feng, L. Yan, H. Zang and Y. Li, *J. Mater. Chem. A*, 2017, **5**, 765–772.
45 Q. Song, X. Qiao, L. Liu, Z. Xue, C. Huang and T. Wang, *Chem. Commun.*, 2019, **55**, 965–968.
46 L. Castanheira, W. O. Silva, F. H. B. Lima, A. Crisci, L. Dubau and F. Maillard, *ACS Catal.*, 2015, **5**, 2184–2194.